Optics Letters

Experimental demonstration of a tunable photonic hook by a partially illuminated dielectric microcylinder

Igor V. Minin,[1,2] Oleg V. Minin,[1,2] Cheng-Yang Liu,[3,*] Hao-De Wei,[3] Yury E. Geints,[4] and Alina Karabchevsky[5]

[1]Tomsk Polytechnic University, Tomsk, 634050, Russia
[2]Tomsk State University, Tomsk, 634050, Russia
[3]Department of Biomedical Engineering, National Yang-Ming University, Taipei City, Taiwan
[4]V.E. Zuev Institute of Atmospheric Optics SB RAS, 1 Zuev Square, Tomsk, 634021, Russia
[5]School of Electrical and Computer Engineering, Ben-Gurion University of the Negev, Beer-Sheva, 8410501, Israel
*Corresponding author: cyliu66@ym.edu.tw

Received 8 July 2020; revised 28 July 2020; accepted 30 July 2020; posted 31 July 2020 (Doc. ID 402248); published 31 August 2020

In this Letter, we report the experimental observations of a tunable curved photonic nanojet (photonic hook) generated by a 5 μm polydimethylsiloxane microcylinder deposited on a silicon substrate and illuminated by 405 nm laser beam. A moveable opaque aluminum-mask is mounted in front of the microcylinder implementing partial illumination and imparting spatial curvature to the photonic nanojet. Experimental results of main parameters (tilt angle, width, and intensity) of emerging photonic hooks exhibit close agreement with numerical predictions of the near-field optical structures. The experimentally measured full widths at half-maximum of photonic hooks are 0.48λ, 0.56λ, and 0.76λ for tilt angles of $\theta = 0°$, 5.7°, and 20.1°, respectively. Photonic hooks possess great potential in complex manipulation such as super-resolution imaging, surface fabrication, and optomechanical manipulation along curved trajectories.

https://doi.org/10.1364/OL.402248

From ancient times, it has been well-known that light propagates in straight lines named rays [1]. However, in 2007, the self-accelerating Airy beams, which do not propagate as rays but rather as curved beams, were proposed and experimentally shown in optics [2,3]. The Airy-like accelerating curved beams exhibit many very important features [4]. In 2015, an original type of subwavelength curved beam named the photonic hook (PH) was proposed based on the physical principles of photonic nanojet (PNJ) formation [5–7]. The optical properties of the PNJ are a function of particle geometry [8,9], refractive index contrast [7,10], and dimensions [6–10]. Moreover, the size (Mie) parameter q of a dielectric mesoscale particle should lie in the range of $q \sim (2 \ldots 20)\pi$ [7], where $q = 2\pi r/\lambda$, r is the radius of the particle, and λ is the incident wavelength.

As a striking example of PH, optical field distribution near a dielectric trapezoid particle with broken symmetry was theoretically studied and experimentally verified [11–13]. A similar PH effect can be observed while using other types of Janus particles with a full illuminating beam [14,15]. Worthwhile noting, the PH emerged from a cuboid with broken symmetry has a radius of curvature, a lateral size of subwavelength, and no curved sidelobes [16]. The influence of specific illumination conditions (coaxial illumination with the adjustable area and boundary illumination) for spherical $BaTiO_3$ particles with a diameter of approximately 127λ ($q \sim 42\pi$) [17] and SiO_2 microspheres with a diameter of 433λ ($q \sim 144\pi$) [18] (while being out of mesoscale conditions) was considered in the optical waveband. This phenomenon is similar to a cylindrical lens with a decentered aperture under normal illumination because of the large spherical aberration [19,20]. The PH formation using a glass cuboid embedded in a structured dielectric cylinder was studied numerically [21]. Furthermore, two PHs were observed by the specially designed five-layer dielectric cylinder [22]. Most of these known solutions usually require specially designed particles or complex processing methods, which limits the further development of this type of curved beam. In this Letter, we experimentally report the direct imaging of curved PNJs created by a mesoscale particle of cylindrical shape ($q \sim 12\pi$) while partially blocking an incident light by an amplitude metal mask. To this end, we study the key parameters of the PH such as lateral full width at half-maximum (FWHM), tilt angle, and maximal intensity depending on the variation of the mask height.

The schematic of the studied system with the definition of curvature for a PNJ is shown in Fig. 1(a). Figure 1(b) shows the schematic 3D view of the system generating curved localized beams. We studied numerically the production capability of the curved PNJ using a dielectric microcylinder illuminated by a laser beam under different height h of the metallic mask. This laser beam is a quasi-plane wavefront since the Gaussian beam with a waist of 1 mm is much bigger than 5 μm diameter of dielectric microcylinder. We illuminate the cylinder with the incident wavelength $\lambda = 405$ nm. The metal (Al) mask is placed in front of the cylinder as close as about 1 μm. The curvature of the PH is defined by the tilt angle θ [11–13]. To simulate

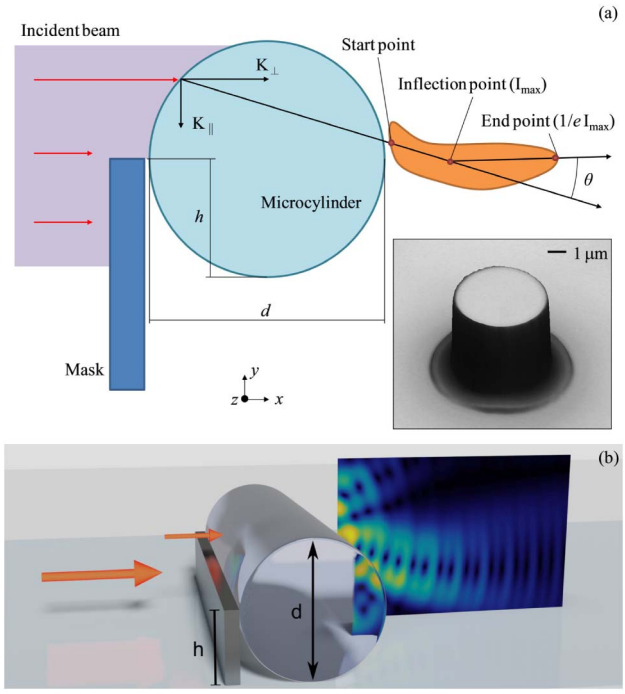

Fig. 1. (a) Schematics description of curvature for a photonic hook. The insert shows the microphotograph of the 5 μm dielectric microcylinder. (b) Schematic render of the studied system.

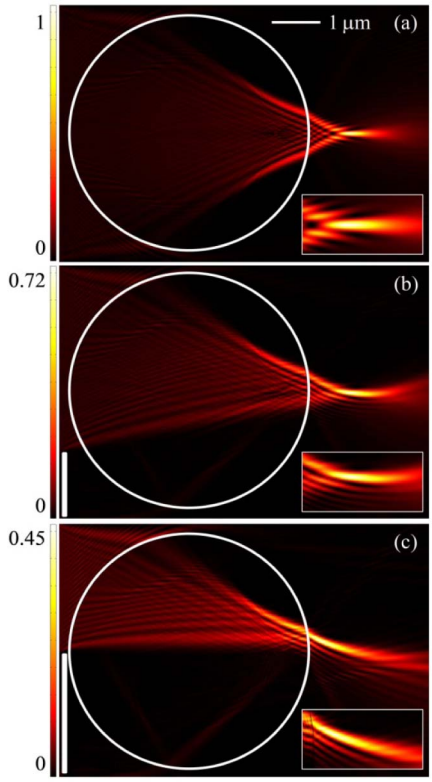

Fig. 2. Numerical results of normalized intensity maps for the dielectric microcylinder with metallic mask at (a) $h = 0$, (b) $h = 0.25\,d$, and (c) $h = 0.5\,d$. The incident wavelength for these calculations and experiments is 405 nm. Zoomed-in PH is shown in insets.

the near-field structure of localized electromagnetic waves, we use the finite-difference time-domain method with perfectly matched layer boundary conditions [23]. We have built several numerical models of 5 μm microcylinder coupled with a metal mask at different h values for quantifying the influence of the illuminating beam width.

To reveal the curvature changes of the PHs, the field intensity distributions at several key h values by numerical simulations are illustrated in Fig. 2. The case with $h = 0$ corresponds to the classical PNJ for a dielectric microcylinder. As shown in Fig. 2, the PH's shape and curvature radius can be adjusted by varying mask height. In particular, when comparing Figs. 2(a)–2(c), we noticed that the curvature of the PH changes when the mask height varies from $h = 0$ to $0.5\,d$. The physics of the curved PNJ formation can be explained as follows. The refractive index of cylinder and width of illumination determines the angle of refraction on an interface via the generalized Snell's law [24]. Part of the illuminating beam, determined by the mask height, is refracted first on the front surface of the cylinder. Then, the light beam inside the cylinder is refracted a second time when it exits from the shadow surface of the cylinder [see Fig. 1(a)]. If the width of the illuminating beam is less than the cylinder diameter, the components of the wave vector $K_{\|}$ do not cancel each other through the local destructive interference [25]. The wave vector $K_{\|}$ is relative to the axis of symmetry of the cylinder, which creates the PNJ curvature profile. On the other hand, the components of the wave vector $K_{\perp}$ determine the length of the PNJ along the propagation direction. Therefore, the local optical fields interfere inside the cylinder, and then the PH can be generated outside the cylinder depending on the width of the illuminating beam.

To experimentally demonstrate the PH phenomenon based on spatially limited illumination, we built a setup shown in Fig. 3(a). It consists of a linearly polarized single-mode diode-pumped solid-state laser. We use a variable density filter to modify the intensity of the incident laser beam. The metal mask and substrate (silicon wafer with refractive index $n_w = 5.567 + 0.386i$) [26] are mounted on two independent stages. The linear motorized stages (SigmaKoki SGSP20-85) have 100 nm lateral resolution in both x and y directions for positioning the metallic mask and substrate. An objective (Olympus MPlan 100x) with numerical aperture of 0.9 is mounted on a piezoelectric actuator (SigmaKoki SFS-OBL-1) with 10 nm resolution in the z direction. The piezoelectric actuator in the z direction was used to define the focal plane of interest with the precision of tens of nanometers and successfully imaged the PH via a complementary metal oxide semiconductor (CMOS) camera (Whited UC-1800). All imaging systems are located in a light-controlled darkroom for preventing any effect of the background noise.

We fabricated the dielectric microcylinder with refractive index $n = 1.41$ and a height of 6 μm out of polydimethylsiloxane (PDMS) using conventional photolithography and a replica molding process [27]. The PDMS microcylinder was then placed on the silicon wafer. The material of the metallic mask is aluminum, and the mask width is about 100 μm. A laser scanning digital microscope (LSDM) was used to measure the surface profile of the PDMS microcylinder [28]. The LSDM image of a single PDMS microcylinder is presented in the inset of Fig. 1(a). The top and the bottom diameters of the microcylinder were measured as 4.92 μm and 5.31 μm, respectively.

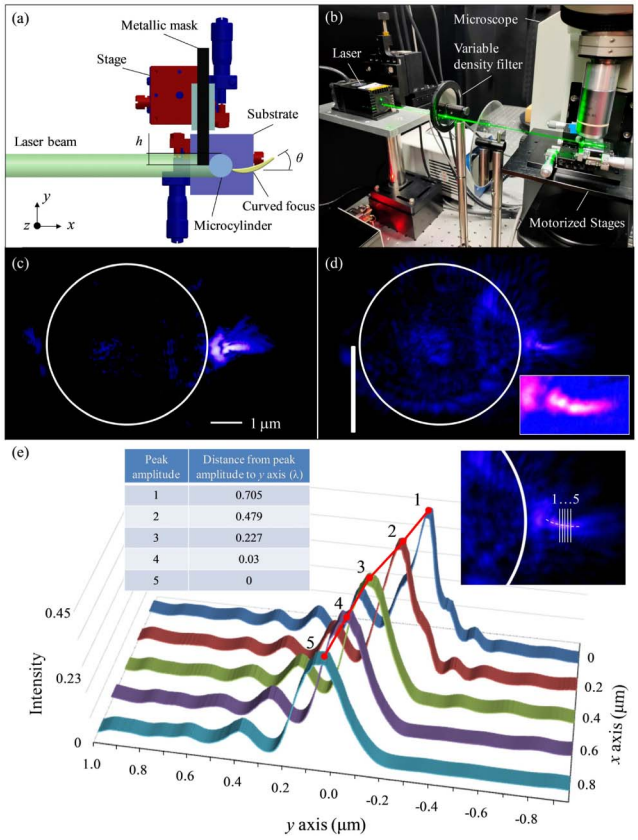

Fig. 3. (a) Schematic diagram of the curved focus generated by a dielectric microcylinder with a metallic mask. (b) Experimental configuration of the scanning microscope system. Experimental raw images of intensity maps for the dielectric microcylinder with metallic mask at (c) $h = 0$ and (d) $h = 0.5\,d$. The incident wavelength is 405 nm. The insert indicates the enlargement of the PH. (e) Experimental cross sections of the observed curved focus at $h = 0.5\,d$. The insert indicates the positions of serial cross sections. The table inset shows the offset distance from each peak amplitude to y axis.

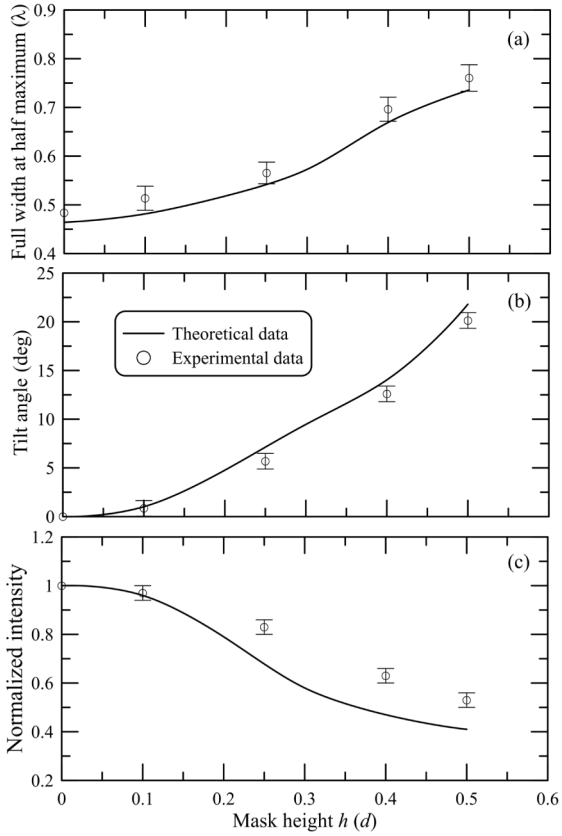

Fig. 4. (a) Full width at half-maximum, (b) tilt angle, and (c) normalized intensity of the curved focus as a function of the mask height. Each experimental point is an average of 10 separate measurements.

The value of surface roughness for this microcylinder was evaluated as Ra = 16 nm, which indicates a reasonable uniformity in the diameter of PDMS microcylinder.

In the experiment, the PDMS microcylinder is illuminated by a coherent laser beam along the x direction, which is shown in Fig. 3(a). We assemble the scanning optical microscope to capture the experimental raw images [29]. The scanning in the z direction is performed for obtaining clear raw images of the PHs [30]. Figures 3(c) and 3(d) show the experimental results of the PH visualization. By comparison of the results from Figs. 2(c) and 3(d), we notice that the intensity distributions for the numerical and experimental results are in good agreement. In both simulations and experiments, the variation of the PH curvature depends on the mask height. Importantly, by tuning the mask height, the curvature of PNJ is tuned in the y direction.

Figure 4 summarizes the PH curvature and the peak intensity compared to these in the full illumination case ($h = 0$). For evaluating the tilt angle and the FWHM of the PHs, we use the following procedure [11,13]. First, based on the experimentally recorded 2D distributions of PH intensity similar to those in Figs. 1(c) and 1(d), the contour maps at the I_{max}/e level are rendered and then conditionally divided into two parts representing left and right arms of the hook with the inflection point having maximal intensity I_{max}. Next, PH start and end points are selected as the extreme points of both the left and right arms, respectively. If PH distributes across the microcylinder boundary, the start point is the intersection point of the left PH arm and the microcylinder boundary. The left (start-inflection points) and right (inflection-end points) PH arms relative to the direction of radiation incidence are shown in Fig. 1(a). The tilt angle θ is identified as the supplementary angle between the left and the right PH arms. The FWHM is the double distance perpendicular to the propagation direction between I_{max} and the half-maximum point. To measure real length in the experimental images, a standard reticle is used to calibrate the pixel and real length conversion. Figures 4(a) and 4(b) show the FWHM and the tilt angle of the produced PH at the peak amplitude, respectively. The diffraction-limited PH (FWHM $\leqq \lambda/2$) is observed at mask height $h \leqq 0.15\,d$ with a small tilt angle less 2.5° while the maximal field intensity decreases by up to 10%. However, the FWHM of the PH is more than that of a classical PNJ at $h > 0.15\,d$ as well. The mask height has a significant influence on the curvature of the PH. When mask height increases, the tilt angle is on a rising trend. It can be seen that the tilt angle θ of the PH is about 20° at the mask height of $h = 0.5\,d$. The full length of the PH in the case of $h = 0.5\,d$ is about 3 μm, in which the distance between the origin and inflection point is 0.8 μm and the distance between the inflection point and the target point is 2.2 μm. In case there is no mask, the FWHM of the PNJ is less

than half of the wavelength. However, the FWHM of the PH is 0.76λ when the mask height is equal to half of the cylinder diameter. In Fig. 4(c), the peak intensity of the PH decreases as the mask height increases. At $h = 0.5\,d$, the peak intensity has decreased to approximately 0.5, half of its original intensity.

To demonstrate the curvature of the PH, the experimental cross sections of the observed curved focus at $h = 0.5\,d$ are shown in Fig. 3(e). Serial transverse cross sections correspond to serial focal planes along the x axis moving upward by steps of 200 nm. We acquire the cross sections from the raw images in Fig. 3(d) and select five cross sections from the inflection point for better observation, as schematically shown in the inset of Fig. 3(e). When the incident beam illuminates a full surface of the microcylinder, the optical beam will be divided into two branches inside the microcylinder and converge into a PNJ near the shadow surface of the microcylinder [6,7] [see Fig. 2(a)]. For a masked microcylinder, one of the branches inside the microcylinder is blocked by the metallic mask as shown in Fig. 2(c). Only one part of the optical beam inside the microcylinder is refracted on the rear surface of the microcylinder, and then a curved focus area is formed near the shadow surface of the microcylinder. Another key factor to remember is that the wave oscillations of a complete phase cycle inside the microcylinder are irregular due to the asymmetry of illuminating waves by mask apodization, and this is the cause of an optical bending beam. The table inset in Fig. 3(e) shows the offset distance from each peak amplitude to the y axis. It can be seen that the position of the peak amplitude in the region of radiation localization shifts in the transverse direction (y axis) when the distance from the shadow surface of the microcylinder increases in the horizontal direction (x axis). In other words, the localized optical beam is not direct, and the focusing beam is bent to form a PH near the rear surface of the microcylinder. Analysis of experimental data shows that the offset distance of the PH increases 5.5 times in the 1 μm length with increasing mask height from $h = 0.25\,d$ to $h = 0.5\,d$. Thus, increasing the mask height leads to a significant increase in the PH curvature. In terms of tilt angle, a larger h leads to a bigger θ. As one can see, the FWHM of the PH increases as the tilt angle increases. In comparison to the classical PNJ, the spatial resolution of the PHs is worse. However, the advantage of the PH is not in its ultra-high spatial resolution, but rather in its subwavelength bend. The price of increasing the PH curvature is the decrease of the maximum intensity of the focus, as shown in Fig. 4(c).

To conclude, we directly observed experimental images of curved PNJs in the visible light region. The PH can be simply created using a mesoscale cylindrical dielectric particle with an amplitude mask. The PH generation considered in this Letter does not require the manufacture of microparticles with a special shape or complex internal structure. The mesoscale dimensions and simplicity of the PHs are much more controllable for a variety of practical applications. The observed PH generation should be inherent to acoustic, surface waves, and microwaves for interacting with mesoscale symmetric obstacles and asymmetric illumination. The future research can explore the influence of the pulsed laser illumination on the PH parameters [31].

Funding. Russian Foundation for Basic Research (20-57-S52001); Israeli Innovation Authority Funding (69073); Yen Tjing Ling Medical Foundation (CI-109-24); Ministry of Science and Technology, Taiwan (109-2923-E-010-001-MY2); Israel Science Foundation (2598/20), State Contract for the Institute of Atmospheric Optics; Tomsk Polytechnic University Competitiveness Enhancement Program.

Disclosures. The authors declare no conflicts of interest.

REFERENCES

1. L. Novotny and B. Hecht, *Principles of Nano-Optics* (Cambridge University, 2006).
2. G. Siviloglou and D. Christodoulides, Opt. Lett. **32**, 979 (2007).
3. G. Siviloglou, J. Broky, A. Dogariu, and D. Christodoulides, Phys. Rev. Lett. **99**, 213901 (2007).
4. N. Efremidis, Z. Chen, M. Segev, and D. Christodoulides, Optica **6**, 686 (2019).
5. I. V. Minin and O. V. Minin, *Diffractive Optics and Nanophotonics: Resolution Below the Diffraction Limit* (Springer, 2016).
6. A. Heifetz, S. Kong, A. Sahakian, A. Taflove, and V. Backman, J. Comput. Theor. Nanosci. **6**, 1979 (2009).
7. B. Luk'yanchuk, R. Paniagua-Domínguez, I. V. Minin, O. V. Minin, and Z. Wang, Opt. Mater. Express **7**, 1820 (2017).
8. A. Itagi and W. Challener, J. Opt. Soc. Am. A **22**, 2847 (2005).
9. C. Liu and F. Lin, Opt. Commun. **380**, 287 (2016).
10. Y. Geints, A. Zemlyanov, and E. Panina, J. Opt. Soc. Am. B **28**, 1825 (2011).
11. L. Yue, O. V. Minin, Z. Wang, J. Monks, A. Shalin, and I. V. Minin, Opt. Lett. **43**, 771 (2018).
12. I. V. Minin, O. V. Minin, G. Katyba, N. Chernomyrdin, V. Kurlov, K. Zaytsev, L. Yue, Z. Wang, and D. Christodoulides, Appl. Phys. Lett. **114**, 031105 (2019).
13. Y. Geints, I. V. Minin, and O. V. Minin, J. Opt. **22**, 065606 (2020).
14. G. Gu, L. Shao, J. Song, J. Qu, K. Zheng, X. Shen, Z. Peng, J. Hu, X. Chen, M. Chen, and Q. Wu, Opt. Express **27**, 37771 (2019).
15. I. V. Minin, O. V. Minin, L. Yue, Z. Wang, V. Wolkov, and D. Christodoulides, "Photonic hook–a new type of subwavelength self-bending structured light beams: a tutorial review," arXiv:1910.09543 (2019).
16. K. Dholakia and G. Bruce, Nat. Photonics **13**, 229 (2019).
17. F. Wang, L. Liu, P. Yu, Z. Liu, H. Yu, Y. Wang, and W. Li, Sci. Rep. **6**, 24703 (2016).
18. E. Xing, H. Gao, J. Rong, S. Khew, H. Liu, C. Tong, and M. Hong, Opt. Express **26**, 30944 (2018).
19. Z. Cao, C. Zhai, J. Li, F. Xian, and S. Pei, Opt. Commun. **393**, 11 (2017).
20. M. Avendaño-Alejo, L. Castañeda, and I. Moreno, J. Opt. Soc. Am. A **27**, 2252 (2010).
21. J. Yang, P. Twardowski, P. Gérard, Y. Duo, J. Fontaine, and S. Lecler, Opt. Express **26**, 3723 (2018).
22. Y. Huang, Z. Zhen, Y. Shen, C. Min, and G. Veronis, Opt. Express **27**, 1310 (2019).
23. A. Taflove and S. Hagness, *Computational Electrodynamics: The Finite Difference Time Domain Method* (Artech House, 2005).
24. N. Yu, P. Genevet, M. Kats, F. Aieta, J. Tetienne, F. Capasso, and Z. Gaburro, Science **334**, 333 (2011).
25. H. Yang, R. Trouillon, G. Huszka, and M. Gijs, Nano Lett. **16**, 4862 (2016).
26. E. Palik, *Handbook of Optical Constants of Solids* (Academic, 1985).
27. Y. Zhang, C. Lo, J. Taylor, and S. Yang, Langmuir **22**, 8595 (2006).
28. C. Liu and K. Hsiao, Opt. Lett. **40**, 5303 (2015).
29. C. Liu and W. Lo, Opt. Commun. **399**, 104 (2017).
30. P. Ferrand, J. Wenger, A. Devilez, M. Pianta, B. Stout, N. Bonod, E. Popov, and H. Rigneault, Opt. Express **16**, 6930 (2008).
31. M. Spector, A. Ang, O. V. Minin, I. V. Minin, and A. Karabchevsky, Nanoscale Adv. **2**, 2595 (2020).